Coarse-grained simulations of the solution-phase self-assembly of poly(3-hexylthiophene) nanostructures†

Kyra N. Schwarz, Tak W. Kee, and David M. Huang*

Received Xth XXXXXXXXXX 20XX, Accepted Xth XXXXXXXXX 20XX
First published on the web Xth XXXXXXXXXX 200X
DOI: 10.1039/b000000x

Under certain conditions the conjugated polymer poly(3-hexylthiophene) (P3HT) self-assembles into high-aspect-ratio nanostructures (known as nanofibres, nanowires, or nanoribbons) when cooled below its solubility limit in a marginal solvent such as anisole. Such nanostructures are potentially beneficial for organic photovoltaic device performance. In this work, Langevin dynamics simulations of a coarse-grained model of P3HT in implicit anisole solvent are used to study the self-assembly of P3HT nanostructures for polymer chain lengths and concentrations used experimentally to prepare P3HT nanofibres. The coarse-grained model is parametrised to match the local structure and dynamics of an atomistic model with explicit solvent. Nanofibres are also prepared experimentally and characterised by atomic force microscopy and UV-vis spectroscopy. The simulations match the experimental phase behaviour of P3HT in anisole, showing aggregation of P3HT at 293 and 308 K but not at 323 or 353 K. Single-chain simulations at 293 K reveal two distinct nano-scale aggregate morphologies: hairpins and helices. Hairpin aggregates, which are the precursors of nanofibres, are slightly favoured energetically at 293 K for nuclei of the critical size of ≈80 monomers for aggregation. Consequently, chains in multi-chain aggregates adopt the hairpin morphology exclusively in simulations at experimental concentrations at 293 K. The simulated aggregate sizes match experimentally measured nanofibre widths. An estimate of the shift in UV-vis absorption of P3HT due to the change in conjugation length with aggregation in the simulations agrees reasonably well with experiment and shows that most of the spectral red shift that occurs with nanofibre formation is due to increased planarisation of the P3HT chains. In addition to providing insight into the mechanisms of nanofibre formation, the simulations resolve details of the molecular-level organisation of chains in P3HT nanofibres hitherto inaccessible by experiment.

1 Introduction

The nano-scale morphology of conjugated polymers plays a crucial role in the performance of organic electronic devices such as solar cells.[1] The ability to control polymer morphology is thus an important step towards the rational optimisation of such devices. Self-assembly is one means of making reproducible nano-scale structures that has considerable practical advantages over other methods for fabricating such structures, such as nanolithography.[2]

Poly(3-hexylthiophene (P3HT) is one of the most widely used polymers in organic photovoltaic devices[3] and is known to self-assemble into nanostructures including high-aspect-ratio nanofibres due to its natural tendency to aggregate in an ordered, quasi one-dimensional fashion.[4–8] These nanofibres (which are perhaps more accurately described as nanoribbons) are typically tens of nanometres wide, a few nanometres high, and up to microns long.[4,6,8,9] Nanofibres can be prepared in a variety of ways,[2] with one common solution-phase technique involving gradually modifying the polymer's solubility so that controlled aggregation occurs, for example by dissolving the polymer in a marginal solvent at heightened temperature and allowing aggregation to occur through a slow cooling process.[6,7] Aggregation can also be induced by using mixed solvents.[2] The unfavourable entropy decrease that occurs as a result of the formation of large assembled molecular structures is overcome by the reduction of less favourable solvent interactions upon aggregation. The anisotropic interactions between monomers along the polymer chain, which include π–π and alkyl side-chain interactions, help to drive the self-assembly of high-aspect-ratio nanostructures.

One significant practical reason for the strong interest in high-aspect ratio conjugated polymer nanostructures is their potential for improving the performance of organic solar cells, in which conjugated polymers are often the electron donor material in a typically disordered donor/acceptor mixture, by providing an optimal morphology for exciton and charge transport. These nanostructures can improve efficiency by provid-

† Electronic Supplementary Information (ESI) available: Atomistic and coarse-grained force fields and bond length, bond angle, dihedral angle, and non-bonded distributions of poly(3-hexylthiophene) (P3HT) in anisole; experimental UV-vis absorption spectra of non-aggregated and nanofibre P3HT. See DOI: 10.1039/b000000x/

School of Chemistry & Physics, The University of Adelaide, SA 5005, Australia. Tel: +61-8-8313-5580; E-mail: david.huang@adelaide.edu.au

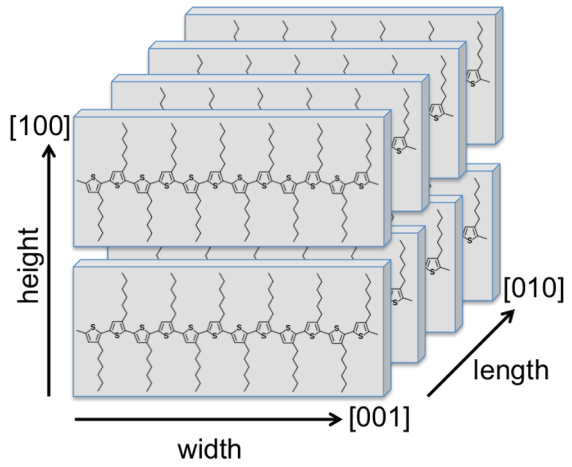

Fig. 1 Schematic of the molecular structure of a P3HT nanofibre.

ing short pathways on the order of the exciton diffusion length of ∼10 nm for light-induced electronic excitations (excitons) to diffuse to donor/acceptor interfaces, by providing long continuous pathways for holes and electrons produced at these interfaces to migrate to the electrodes, and by improving charge-carrier mobilities.[10–13]

Experimental techniques such as grazing incidence x-ray diffraction, electron diffraction, and transmission electron microscopy have provided important insight into the structure of molecular-level structure of P3HT nanofibres.[4,8,14] For example, it is known that the longest axis of a P3HT nanofibre corresponds to the π-stacking direction ([010] direction), the second longest axis corresponds to the direction of the polymer repeat units ([001] direction), and the shortest axis corresponds to the direction of the alkyl side chains ([100] direction), as shown in Fig. 1. Typical nanofibre lengths of hundreds to thousands of nanometres, widths of tens of nanometres, and heights of 3–7 nanometres[14] suggest thousands of π-stacked layers along the [010]-axis, tens of thiophene repeat units along the [001]-axis, and 2–4 chains along the [100]-axis, given experimentally measured unit cell spacings of $b = 0.38$ nm, $c = 1.68$ nm, and $a = 0.78$ nm, respectively.[14]

But much is still not known about the molecular-level organisation of the chains within P3HT nanofibres or the mechanism by which they self-assemble. The substantially larger contour length of the polymer chains (>100 nm for typical molecular weights) compared with the nanofibre width of tens of nanometres means that the chains must loop back on themselves in the nanofibre in the [001] direction. The particular arrangement of individual chains when they loop back on themselves (*e.g.* do different segments end up in the same or different (100) or (010) planes?) and the nature of the loops (e.g. their radius of curvature) are difficult, if not impossible, to resolve experimentally. Given the significant impact that polymer conformation has on the electronic properties of conjugated polymers such as P3HT,[15] insight into these issues would be beneficial.

Computer simulation models can help to clarify the structure and dynamics of self-assembly of conjugated polymer nanostructures in solution. So far almost all molecular-level computational studies of P3HT have used models in which the polymer chains are described in atomistic detail.[16–22] However, such atomistic simulations are only readily feasible for polymer chain lengths and time scales smaller than those needed to observe the self-assembly of structures larger than a few nanometres. Furthermore, none of these studies has addressed the structure or dynamics of P3HT in solution, let alone the self-assembly of P3HT nanostructures.

A more computationally feasible alternative that can accurately capture many of the molecular-level details of an atomistic simulation model is to use a systematically coarse-grained (CG) model, in which each CG site represents a collection of atoms and in which the interactions between CG sites are parametrized to reproduce the local structure[23] or forces[24] in the atomistic model. Systematically coarse-grained models have been developed in the past to describe the morphology of P3HT and P3HT/fullerene mixtures in the liquid state.[25–27] However, such methods have never been applied to study P3HT nanostructure formation in solution.

In this paper, a coarse-grained model of P3HT in implicit anisole solvent is systematically parametrised from an atomistic model with explicit solvent and is used to model the aggregation of P3HT nanostructures in anisole, a marginal solvent, using classical Langevin dynamics simulations for experimentally relevant polymer chain lengths and solvent concentrations. High-aspect-ratio P3HT nanostructures, namely nanofibres, are also prepared experimentally and are characterised by atomic force microscopy (AFM) and UV-vis absorption spectroscopy. The phase behaviour and structural properties of P3HT in the coarse-grained simulations are compared with experiments, while analysis of the simulation results is used to provide insight into the self-assembly process and molecular-level structure of P3HT nanofibres.

2 Computational methods

2.1 Atomistic simulation model

The atomistic model of P3HT (chemical structure given in Fig. 2) was adapted from the P3HT model previously developed by Huang et al.,[25] which was in turn adapted from a model of tetrathiophene.[28] The tetrathiophene model uses equilibrium bond lengths and angles and partial charges from quantum density functional theory (DFT) calculations and takes the rest of its parameters (except for the inter-monomer

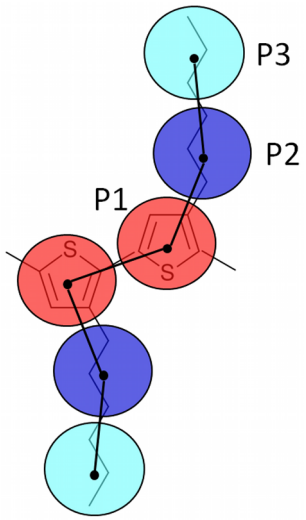

Fig. 2 Chemical structure of P3HT with coarse-grained sites depicted and labelled.

torsional potential) from the widely used OPLS-AA force field.[29] This model agrees well with experiments for structural and thermodynamic properties of tetrathiophene, including the density, crystal structure, and heat of sublimation. Parametrisation of the atomistic P3HT model essentially involved adding a hexyl side chain (with parameters taken directly from the OPLS-AA force field) to this tetrathiophene model, as well as replacing the inter-monomer torsional potential obtained from DFT calculations of a thiophene dimer with a DFT-derived potential for substituted thiophene oligomers,[30] which accounts for the higher torsional barriers due to extended electron delocalisation in conjugated oligomers compared with dimers or small molecules.[30] For similar reasons, a torsional potential from the OPLS-AA force field, which was parametrised based on the properties of small molecules, was not used.

The procedure used to parameterise the P3HT model is described in detail in Ref. 25. The P3HT model used here differs in two respects from that in Ref. 25 and follows more closely the OPLS-AA force field. First, OPLS-AA parameters[31] were used for the dihedral potentials that maintain planarity of the thiophene ring, since the potentials used in Ref. 25 were found to allow unphysical out-of-plane ring motion, which resulted in simulated P3HT oligomers in which the most probable thiophene ring configuration was non-planar. Second, due to the changes to the intra-ring dihedral potentials, it was necessary to reparametrise the inter-monomer torsional potential. Following the procedure in Ref. 25, this potential was fitted to the inter-monomer torsional potential from quantum DFT calculations of an isolated 3-methylthiophene 14-mer.[30] The only difference between the models for 3-methylthiophene and 3-hexylthiophene was the length of the alkyl side chains in the two molecules. The atomistic P3HT model parameters and the fitting of the inter-monomer torsional potential are given in the Supplementary Information. The density of P3HT monomers at 298 K and 1 atm (0.933 ± 0.002 g/mL) simulated using the model in a 1-ns simulation of 256 monomers at constant temperature and pressure agrees well with experiment (0.936 g/mL).[32] To model anisole, the OPLS-AA force field[29,31,33] was used without modification.

All atomistic and coarse-grained simulations were carried out for regioregular P3HT (rr-P3HT) using the LAMMPS molecular dynamics (MD) simulation package.[34] VMD was used for visualisation.[35] Atomistic simulations of monomers in anisole and of decamers in anisole were carried out for 6 ns and 22 ns respectively at constant temperature (353 K) and pressure (1 atm) using a Nosé-Hoover thermostat and barostat (NPT ensemble). Carbon–hydrogen bond distances were constrained using the SHAKE algorithm[36] and long-range electrostatic interactions were calculated using the particle–particle particle–mesh (PPPM) method.[37,38] Non-bonded van der Waals interactions, modelled using the Lennard-Jones potential, were truncated and shifted to zero at a cut-off distance of 12 Å. Simulations were carried out in a cubic simulation box with periodic boundary conditions using a time step of 2 fs. Initial configurations consisted of randomly positioned and oriented molecules, with an inter-monomer dihedral angle distribution chosen from a Boltzmann distribution of the inter-monomer torsional potential. Statistical averaging of probability distributions used to parametrise the coarse-grained model was carried out only when the distributions ceased to display systematic variations with time, which typically took $\approx$2 ns. Unless otherwise stated, statistical errors are reported as one standard error in the mean.[39]

2.2 Coarse-grained model parametrisation

Following Ref. 25, each coarse-grained (CG) P3HT monomer unit was modelled as three separate spherical sites, representing (1) the centre-of-mass of the thiophene ring and the centres-of-mass of (2) the first three and (3) last three methyl groups of the hexyl sidechain, as illustrated in Fig. 2. Although the interactions between pairs of spherical sites are isotropic, the overall interactions between monomers are anisotropic and, along with bonded interactions that favour chain conformations consisting of coplanar monomers, can produce anisotropic chain aggregation, as shown in the results below.

Coarse-grained polymers were simulated in implicit solvent using Langevin dynamics[39,40] at constant volume (NVT ensemble) according to the equation-of-motion

$$m_i \ddot{\boldsymbol{r}}_i(t) = \boldsymbol{f}_i(t) - m_i \gamma \dot{\boldsymbol{r}}_i(t) + \boldsymbol{\Gamma}_i(t)\,, \qquad (1)$$

which accounts for the effects of the frictional drag and random collisions of solvent molecules on the polymer chains. Here, m_i and $\boldsymbol{r}_i$ are the mass and position respectively of particle i, $\boldsymbol{f}_i = -\nabla_i U(\{\boldsymbol{r}^N\})$ is the conservative force acting on particle i due to the total CG potential energy U, γ is the friction coefficient, and t is the time. The random force $\boldsymbol{\Gamma}_i$ acting on particle i satisfies $\langle \boldsymbol{\Gamma}_i(t) \rangle = 0$ and $\langle \boldsymbol{\Gamma}_i(t) \boldsymbol{\Gamma}_j(t') \rangle = 2\gamma k_B T m_i \delta_{ij} \delta(t-t')$.

The interactions between CG P3HT sites that determine the potential energy U were optimised by the iterative Boltzmann inversion (IBI) method,[23,41] following the procedure described in Ref. 42, to match the radial distribution functions (RDFs) between non-bonded sites and bond, angle, and dihedral distributions of an equivalent atomistic system (i.e. a system with the same number and length of polymer chains and average system volume). In this way, the interactions between CG sites were parametrised to give an accurate representation of the local structure in the atomistic simulations. The bonded CG interactions were fitted to analytical functions, while the non-bonded interactions were fitted by a tabulated numerical potential. Because the solvent molecules are not explicitly simulated in the CG model, the resulting non-bonded CG interactions are effective solvent-mediated interactions. Due to the statistical-mechanical relationship between the RDF and the free energy versus distance between a pair of particles in the presence of other particles such as solvent,[43] optimisation of the non-bonded CG interactions to match the atomistic RDFs produces CG interactions that include contributions from many-body solvent–solvent and solvent–polymer correlations and therefore also solvation entropy and enthalpy, even though explicit solvent degrees of freedom are integrated out. The potential functions and optimised parameters in the CG model are given in the Supplementary Information.

The bonded and non-bonded CG interactions were optimised respectively in simulations of 4 decamers in anisole and of 40 monomers in anisole. Both simulations were carried out at 353 K and a concentration of 5.4-wt%, for which 1134 anisole molecules were used. Non-bonded and bonded interactions within the individual monomers were first optimised in the monomer simulations. These parameters were then fixed and the remaining bonded interactions were optimised in the decamer simulations. The previously optimised interactions gave good agreement after all interactions had been optimised. Decamers were used to parametrise the bonded interactions, as these have previously been shown to accurately represent the behaviour of long-chain polymers in the coarse-graining procedure.[44] The density of the constant-volume CG systems was set to the average density of the corresponding 1-atm constant-pressure atomistic system. The average volume of the monomer and decamer simulations was $(6.09\ \text{nm})^3$ and $(6.08\ \text{nm})^3$ respectively. These average box dimensions were significantly larger than the sum of the contour length of a decamer and the Lennard-Jones cut-off distance. The time step in the CG simulations was 8 fs. As an illustration of the matching of the atomistic and CG structural distributions, the atomistic and CG RDFs and optimised CG pair potentials for the non-bonded interactions are shown in Fig. 3. The remaining distributions and optimised CG potentials for bonded interactions are given in the Supplementary Material.

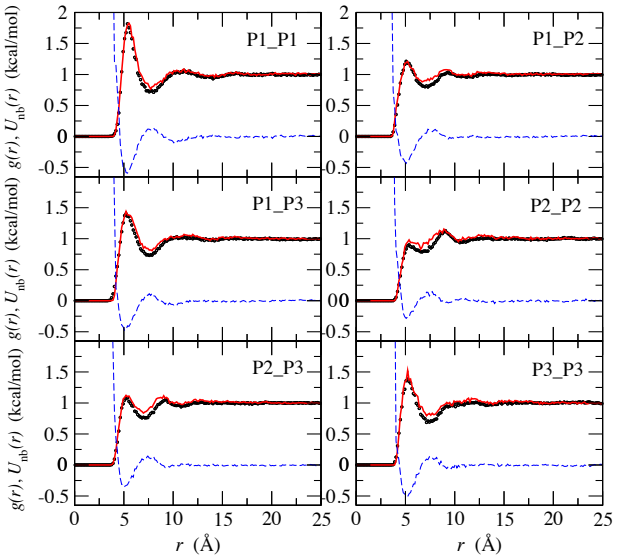

Fig. 3 Radial distribution functions of non-bonded sites from a constant NPT simulation of 40 P3HT monomers and 1134 anisole molecules (5.4-wt% P3HT) at 353 K and 1 atm (circles) and from a constant NVT simulation of the equivalent CG system (solid lines) using optimised CG interaction potentials (dashed lines). Site type definitions are given in Fig. 2.

To match the dynamics in the atomistic and CG simulations, the Langevin dynamics friction coefficient γ was set to $(180\ \text{fs})^{-1}$ in the CG simulations so that the mean squared displacement (MSD) of the monomer centre-of-mass versus time, $\langle r^2(t) \rangle$, was the same in the atomistic and CG simulations of P3HT monomers, as shown in Fig. 4. This value of γ corresponds to conditions of high friction and is consistent with values derived previously for Langevin dynamics of CG models of polymers in implicit solvent[45,46] using the same method of matching the MSD in atomistic and CG simulations of monomers. This value is close to the limit of what can be used with an 8-fs time step using the Langevin dynamics algorithm[40] employed by our CG simulations, which requires simulation time steps much smaller than $1/\gamma$, but alternative algorithms[47] exist that circumvent this limitation.

2.3 Mesoscale coarse-grained simulations

Langevin dynamics simulations of the parametrised coarse-grained model were carried out for the P3HT chain lengths

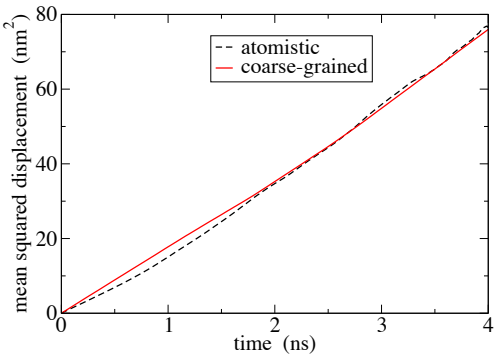

Fig. 4 Mean squared displacement of monomer centre-of-mass vs time from a constant NPT simulation of 40 P3HT monomers and 1134 anisole molecules (5.4-wt% P3HT) at 353 K and 1 atm (dashed line) and from a constant NVT simulation of the equivalent CG system (solid line) with friction coefficient $\gamma = (180\ \text{fs})^{-1}$.

(300 monomers $\approx$ 50 kDa) used experimentally to prepare P3HT nanofibres in anisole in Section 3. Under these conditions, microsecond time-scale simulations were required to observe aggregation of the P3HT chains at room temperature (293 K). Eight separate 6-μs simulations of a single 300-monomer chain in a $(129\ \text{nm})^3$ box were carried out at 293 K, with each simulation starting from a different initial configuration in which the inter-monomer dihedral angles were selected from a Boltzmann distribution of the inter-monomer torsional potential. Two separate large-scale simulations of systems of sixteen 300-monomer chains were simulated in a $(2200\ \text{nm})^3$ box at the solution concentration (0.05 wt%) used experimentally to prepare P3HT nanofibres. The initial configurations consisted of randomly positioned and oriented molecules, with Boltzmann-distributed inter-monomer dihedral angles. The simulations were each run for $\approx$4 μs at 293 K to mimic the experimental conditions for self-assembly of nanofibres upon cooling to this temperature.

For comparison, single-chain and large-scale simulations of equivalent systems were also carried out for several other thermodynamics conditions. Two 12-μs single-chain simulations were undertaken at each of 323 and 353 K and one 12-μs single-chain simulation was carried out at 308 K. The first two temperatures are above the temperature of $\approx$35°C = 308 K at which P3HT started to form nanofibres in anisole in the experiments in Section 3, based on the observed aggregation-induced colour change of the solution that occurred upon cooling. The last temperature is at the onset temperature for nanofibre formation. Previous nanofibre experiments using the same preparation method but with half the P3HT concentration in anisole and a slightly different cooling rate found a similar temperature for nanofibre formation by monitoring the change in absorbance of the solution at 596 nm.[6]

Large-scale sixteen chain simulations were also carried out for 3.9 and 0.6 μs, respectively, at 353 K and at 293 K using pair potentials that were reduced by 10% from those parametrised for P3HT in anisole, i.e. by multiplying all pair potentials in the coarse-grained model of P3HT in anisole at all distances by 0.9. The latter simulation was carried out to mimic P3HT in a better solvent than anisole in which P3HT does not aggregate at room temperature, in order to investigate the impact of aggregation in anisole at 293 K on P3HT morphology, since reducing the polymer–polymer pair potentials in the implicit solvent model is equivalent to making polymer–solvent interactions more favourable.

3 Experimental methods

3.1 P3HT nanofibre preparation

Regioregular poly(3-hexythiophene-2,3-diyl) (P3HT) was obtained from Rieke Metals, (molecular weight (M_w) = 50 kDa, regioregularity 90–94%). Anisole (Merck, Germany) was used as a solvent in which P3HT was marginally soluble.

Using the same approach as Samitsu *et al.*,[6] P3HT nanofibres were prepared by the whisker method,[4] a reliable process for forming very high-aspect-ratio nanostructures. P3HT (1 mg) was dissolved in anisole (2 g) to make a 0.05-wt% solution. The solution was heated under agitation to 80°C to achieve complete dissolution. Stirring was stopped and the solution was gradually cooled at a controlled rate of 20°C/hour to room temperature, whilst protected from ambient light and heat. The nanofibre solution was used within several days of preparation.

3.2 P3HT nanofibre characterisation

Solution-phase absorption spectra were collected on a Cary 5000 UV-Vis-NIR spectrophotometer (Varian) using a 1-cm quartz cuvette. The nanofibre spectrum was measured in anisole and compared with that of uncollapsed P3HT dissolved in HPLC grade tetrahydrofuran (Scharlau, Spain), a moderately good solvent for P3HT.

For atomic force microscopy (AFM) characterisation, nanofibres were deposited on SiO_2/Si substrates by spin-coating from anisole at $\approx$3000 rpm in air (after diluting the solution to 0.01 wt%) until residual solvent had evaporated. AFM was performed in air with a NT-MDT Ntegra Solaris AFM+SNOM operating in tapping mode. Imaging was performed using a silicon cantilever with a spring constant of 0.2 N/m, for which the amplitude was carefully adjusted in order to obtain clear images. The height and width measurements of the nanofibres were obtained from cross-sectional AFM images obtained perpendicular to the long axis of the nanofibre. The width of a nanofibre was determined as the full width at half maximum of the cross-section.

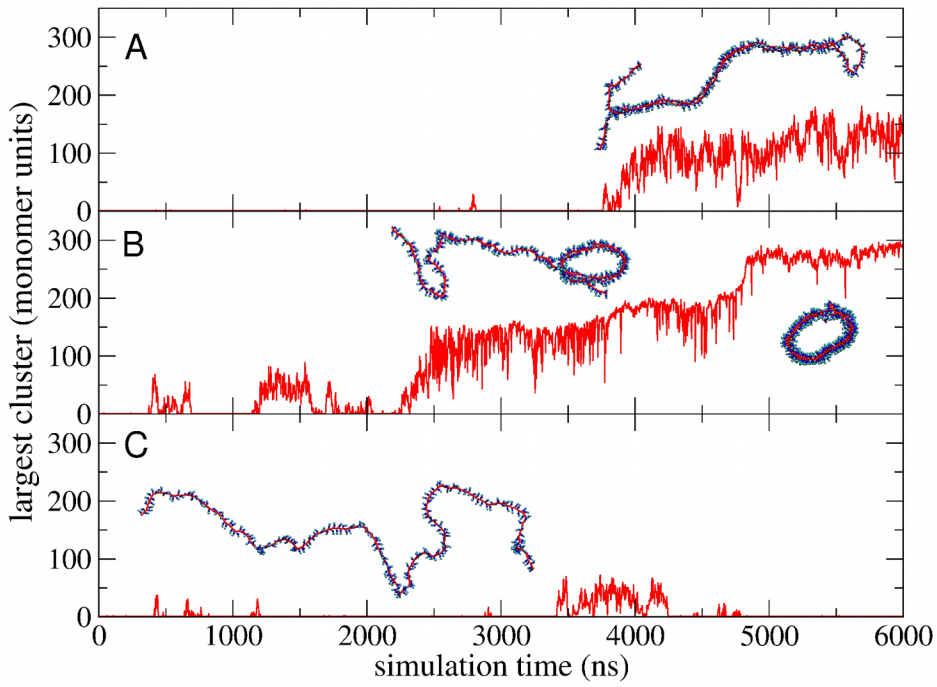

Fig. 5 Size of largest cluster versus time for single-chain aggregates from simulations at 293 K where the final structure was (A) a hairpin (B) a helix and (C) an uncollapsed chain.

4 Results and discussion

4.1 Single-chain coarse-grained simulations

In the single-chain coarse-grained simulations, which are effectively at infinite dilution since the simulation box is large enough that the chain cannot interact with itself, the 300-monomer P3HT chains were found to aggregate in anisole at 293 K on the microsecond time scale to form two distinct nano-scale structures: "hairpins", in which the chain folds back on itself once or twice to form two or three π-stacked layers, and "helices", in which the chain forms a spiral of diameter 5–8 nm of multiple π-stacked layers. Of the eight chains simulated at this temperature, three were observed to form helical structures, three folded into hairpin structures, and two remained unaggregated at the end of 6 µs.

Fig. 5 illustrates the aggregation dynamics of the single chains in terms of the largest cluster of monomers in the system for three of the simulations at 293 K in which the final structure was a hairpin, a helix, and an uncollapsed chain, respectively. Two monomers were deemed to be part of the same cluster if their centres-of-mass were closer than 7 Å and if they were not directly bonded to one another. The results in Fig. 5 (and those from the other five simulations that are not shown) suggest a critical cluster size of around 80 monomers to nucleate a stable aggregate: the chains form transient clusters of up to 80 monomers that fall apart on the sub-µs time scale, but clusters that exceed the critical size do not come apart on the time scale of the simulations. This result is consistent with experimental evidence that poly(3-alkylthiophenes) with less than 60–70 monomers per chain do not form nanofibres.[2]

Fig. 6 shows the total non-bonded pair potential energy and total bonded (bond, angle, dihedral, and improper dihedral) potential energy of the system versus cluster size averaged over all of the simulations forming hairpin and helical aggregates. The total bonded potential energy in Fig. 6 is the same for both aggregate types and decreases slightly with increasing aggregation, mainly due to a decrease in the dihedral energy as a result of the planarisation of the polymer backbone that occurs with aggregation. The total non-bonded pair potential energy, on the other hand, decreases substantially with cluster size for both the hairpin and helical structures. For clusters smaller than the apparent critical cluster size of ≈80, the pair energy for a hairpin aggregate is significantly more negative than that for a helical aggregate. This result suggests that nucleation of hairpin aggregate structures may be more favourable than nucleation of helices. This hypothesis is borne out by the results of the multi-chain simulations (discussed below), in which the multi-chain aggregates that were formed at 293 K consisted exclusively of π-stacked hairpins.

The total pair energy of the helical aggregates does become more negative than that of hairpin aggregates for cluster sizes

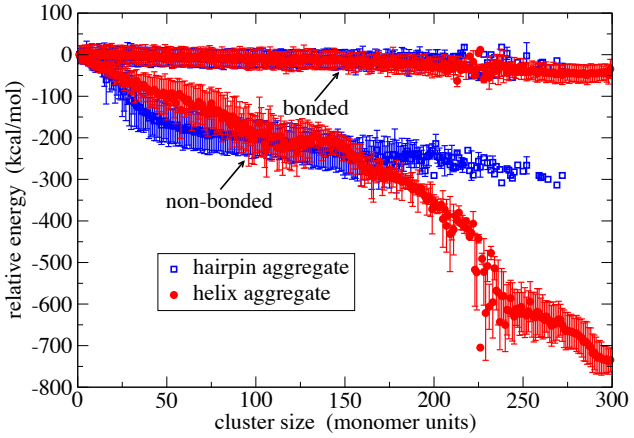

Fig. 6 Total non-bonded and bonded potential energy versus largest cluster size (relative to the average energy for a cluster size of one) from simulations at 293 K for single-chain aggregates with final structures of hairpin and helix morphology. (Error bars are one standard deviation.)

larger than ≈160 monomers, as the helix forms multi-layer π-stacks in which a monomer is able to interact strongly with monomers in more than one adjacent layer. But this energetic advantage of the helical structure in single-chain aggregates should not be significant in multi-chain aggregates, in which hairpins are also able to form multi-layer π-stacked aggregates. There is experimental evidence that P3HT forms helical aggregates under certain conditions: AFM measurements of P3HT aggregates formed by adding hexane to a chloroform solution of P3HT found disk-shaped particles with a diameter of 3–5 nm,[48] consistent with the diameters of the P3HT helices in our simulations. Our AFM measurements also show evidence of circular nanometre-sized objects that could have been helices, but these objects were difficult to characterise.

The analysis given above of the propensities of aggregates to form hairpins or helices does not account for the configurational entropy of the polymer chain, which is expected to be similar for the two aggregate types at a given cluster size or, if anything, be more favourable for hairpins. Assuming for the sake of simplicity that the aggregated part of the chain has no internal configurational degrees of freedom, the configurational entropy of the aggregating chain can be approximated as that of a chain of reduced length equal to the total number of monomers minus the number of monomers in the aggregate, regardless of whether aggregation occurs from the chain end (in the case of helices) or from the chain centre (in the case of hairpins). In reality, the aggregated chain segments do exhibit some flexibility, with hairpins more flexible than the tightly wound helices, indicating a higher entropy for hairpins compared with helices for a given cluster size that would further favour hairpin formation over helix formation.

While P3HT aggregation was observed in the single-chain simulations at 293 K, as well as in the single-chain simulation at 308 K, no aggregation occurred at 323 or 353 K, even after 12 µs. This result agrees with our experimental observations that 0.05-wt% P3HT in anisole only form nanofibres upon cooling below around 35°C = 308 K, based on the aggregation-induced colour change of the solution from orange to purple that occurs as nanofibres self-assemble.

The conformation of the P3HT polymer chains at 323 and 353 K was characterised in terms of the radius of gyration R_g and persistence length l_p. The radius of gyration is defined by

$$R_g^2 = \frac{1}{2N^2}\sum_{i=1}^{N}\sum_{j=1}^{N} r_{ij}^2, \qquad (2)$$

where N is the number of monomers in the chain and r_{ij} is the distance between the centres-of-mass of monomers i and j. The persistence length is given by the decay in the orientational correlation function

$$\langle \cos\theta(l)\rangle \sim \exp(-l/l_p), \qquad (3)$$

where $\cos\theta(l)$ is the angle between inter-monomer bond vectors for bonds separated by a distance l along the contour of the chain.[49] The average radius of gyration $\langle R_g\rangle$ from the simulations of single P3HT chains in anisole at 323 and 353 K was 14.9 ± 1.3 nm and 15.3 ± 1.0 nm, respectively. The persistence length at these temperatures was 6.4 ± 0.3 nm and 6.1 ± 0.2 nm (or 16.7 ± 0.9 monomers and 15.9 ± 0.5 monomers), respectively. The only experimental data on the radius of gyration and persistence length of P3HT that appear to be available is from light scattering measurements of regiorandom P3HT at 25°C in tetrahydrofuran,[50] a moderately good solvent for P3HT. The radius of gyration from these experiments for a slightly higher molecular weight sample (M_w = 75.4 kDa *cf.* 50 kDa in our simulations) was 16.8 nm and the persistence length was 2.4 ± 0.3 nm. Although direct comparison of these measurements and our simulations is not possible, because of the different temperatures, solvent, and polymer regiogularities and high polydispersity (1.9) of the polymer used in the experiments, our results for regioregular P3HT are consistent with the expectation that regioregular P3HT would be more ordered than regiorandom P3HT and therefore have a higher persistence length.

4.2 Multi-chain coarse-grained simulations

Fig. 7 shows configuration snapshots from coarse-grained simulations that had been run for 3.9 µs of sixteen 300-monomer P3HT chains at experimental (0.05-wt%) concentration in anisole at 293 and 353 K. As was found in the single-chain (infinite dilution) simulations, P3HT aggregates at 293 K (Fig. 7B), whereas it remains as uncollapsed chains

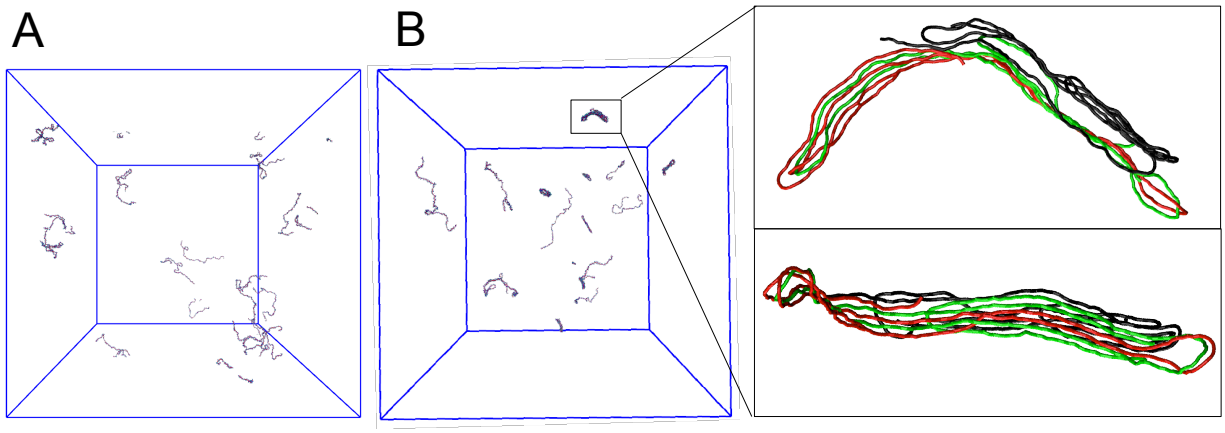

Fig. 7 Configuration snapshots taken after 3.9 μs from coarse-grained simulations of sixteen 300-monomer P3HT chains at 0.05-wt% concentration in anisole at (A) 353 K and (B) 293 K. An example of an aggregated structure is shown magnified on the right viewed from two orientations, in which the vertical direction corresponds to (top image) the [100] axis or alkyl side-chain direction and (bottom image) the [010] axis or π-stacking direction. For clarity, the different polymer chains are coloured differently and the hexyl side chains are not shown.

at 353 K (Fig. 7A), in agreement with the experimental observations that P3HT is fully dissolved at 353 K and forms nanofibres as the temperature approaches 293 K.

Fig. 7B suggests the incipient stages of nanofibre formation. Although some chains in the two 16-chain simulations carried out at 293 K were found to form isolated helix-shaped structures, aggregation of several chains was found to produce ordered multi-chain π-stacked structures in which the individual chains adopt a hairpin-like structure with two to four loops (see the magnified structure in Fig. 7). One three-chain aggregate and 7–10 single-chain aggregates (predominantly hairpin structures) were observed per 16-chain simulation. Some chains did not aggregate during the course of simulations. As discussed above for the single-chain simulations, nucleation of hairpin structures appears to be favoured energetically and is therefore the dominant aggregation pathway observed in the simulations.

The dynamics of self-assembly of such incipient nanofibre structures is illustrated in Fig. 8 for the multi-chain aggregate formed in the simulation at 293 K not shown in Fig. 7. Diffusive motion brings several chains close enough together to interact; chain segments come together, then come apart again due to thermal motion, but if a critical number of monomers come into contact to form favourable π-stacking interactions, a stable nucleus is formed that continues to aggregate; eventually the rest of the chains collapse to become part of the aggregate. The process is analogous to a zipping action, in which chain segments move together to maximise backbone contact starting generally from the chain centre then moving to the more mobile free chain ends. Both 16-chain simulations indicate that the aggregates grow predominantly along the [010] π-stacking direction rather than the [100] alkyl side-chain direction, which is consistent with experimental observations that the long axis of P3HT nanofibres corresponds to the [010] axis.

The three-chain aggregate in Fig. 7 has six π-stacked layers along the [010] axis and two layers along the [100] axis, while that in Fig. 8 also has six π-stacked layers along the [010] axis, but only one layer along the [100] axis. The simulations overestimate slightly the spacing between π-stacked layers, giving a value of around 0.5 nm compared with the experimental value of $b = 0.38$ nm. This is largely due to the approximation of the thiophene ring as a spherical site in the coarse-grained model, which overestimates the steric bulk of the ring in the π-stacking direction. With only one example of a chain forming a second layer along the [100] axis in our simulations (in the aggregate in Fig. 7), there is some uncertainty in our estimate of the layer spacing in this direction; however, the measured values of 1.7 to 2 nm are consistent with the experimental value of $a = 1.68$ nm. Larger configurational fluctuations in our solution-phase aggregates compared with the fully-formed nanofibres measured experimentally in the solid state probably contribute to the overestimates of the a and b spacings.

Depending on the experimental methods and polymer molecular weights used to prepare P3HT nanofibres, a range of nanofibre widths (measured along the [001]-axis) from 15 to 50 nm have been measured.[4,6,8,9,51] Fig. 9 shows the distribution of widths of P3HT nanofibres prepared using the methods described in Section 3. The nanofibre preparation used the same solvent (anisole) and polymer molecular weight (50 kDa) and involved cooling to the same final temperature (293 K) as the simulations, making these measurements most directly comparable with our simulations. The simu-

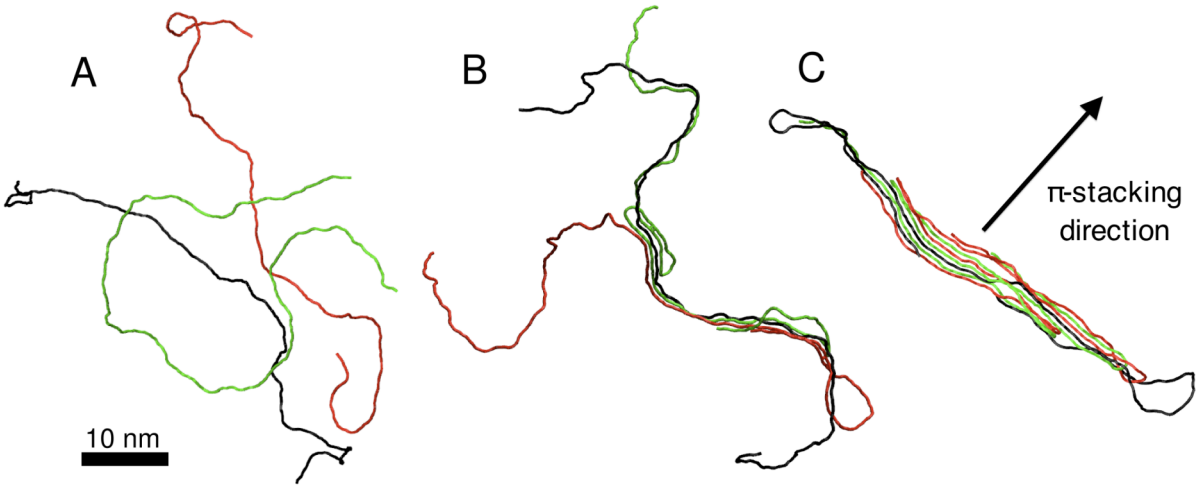

Fig. 8 Self-assembly of three P3HT 300-mers from a simulation of sixteen 300-monomer P3HT chains at 0.05-wt% concentration in anisole at 293 K after (A) 0.06 μs, (B) 1 μs and (C) 4.4 μs. For clarity, the different polymer chains are coloured differently and hexyl side chains are not shown.

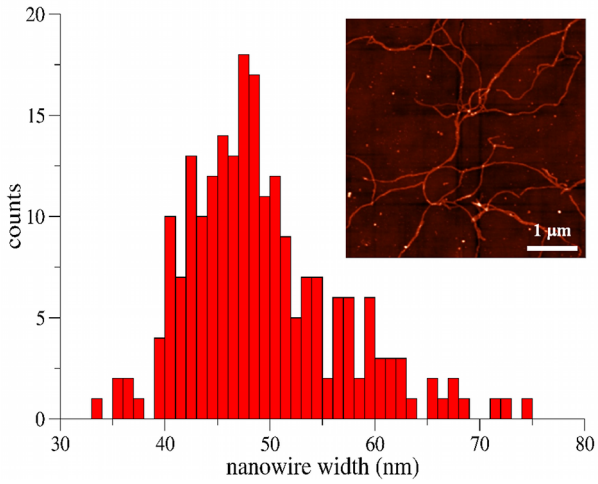

Fig. 9 Experimental width distribution of P3HT nanofibres from AFM images (inset).

lated widths of the multi-chain aggregates in Figs. 7 and 8, measured along the direction parallel to the chain axis, of 36 and 50 nm, respectively, are consistent with the experimentally measured widths from Fig. 9 of 49 ± 13 nm, where the uncertainty has been taken as two standard deviations of the width distribution.

The simulations provide details of the molecular-level organisation of P3HT within incipient nanofibre aggregates that cannot be resolved experimentally. Figs. 7 and 8 show that, in general, the chains lie in the same (100) plane but loop back into different (010) planes in the π-stacking direction. This occurs because the aggregates grow predominantly by π-stacking and not by stacking in the alkyl side chain direction. As a result, the same chain does not generally span different layers in the height (alkyl side chain) direction. The aggregates also exhibit internal loops, where the chains loop back on themselves within the aggregate rather than at the ends. In both the single-chain hairpin structures and multi-chain aggregates observed in the simulations, the diameter of curvature of the end loops formed by the chains was limited to values larger than 2.0 nm (with values up to 3.4 nm measured). The lower bound on the curvature diameter is set by the bending rigidity of the P3HT chain, which is in turn determined by the intra-monomer bonded interactions. With the spacing along the [010] axis ($\approx$0.5 nm) being several times smaller than the minimum curvature diameter, adjacent chain segments in the [010] π-stacking direction in multi-chain aggregates must generally correspond to different chains to minimise the number of monomers in the end loops lacking favourable non-bonded interactions with nearby monomers. On the other hand, single-chain hairpin aggregates, such as those shown in Fig. 5, always exhibit an end loop in which the monomers are not in contact with other monomers.

To further investigate the impact of aggregation on P3HT morphology, a 16-chain simulation was also carried out at 293 K with the strength of the non-bonded interactions between coarse-grained P3HT sites reduced by 10% of the interactions parametrised for P3HT in anisole, which mimics the effect of simulating P3HT in a better solvent than anisole and eliminates aggregation at 293 K, since it is equivalent to changing the temperature for the non-bonded interactions to 326 K, where it was shown above that P3HT does not aggregate in anisole. Although unaggregated P3HT could have also

been simulated anisole at a higher temperature (e.g. 323 K), torsional motion of the polymer backbone would also increase with temperature, making it impossible to deconvolute the effects on structural properties due to thermal motion of the polymer backbone or due to aggregation.

The change in aggregation behaviour on decreasing the interaction strength by 10% also provides an indication of the proximity of the P3HT/anisole system at 293 K to coexistence between the aggregated and non-aggregated phases. This change in the interactions corresponds to a decrease in the well depth in the potential energy curve for the non-bonded pair interactions by just ≈0.05 kcal/mol or $0.1k_BT$ at this temperature, suggesting that the system is close to coexistence at 293 K. This result is consistent with the experimental observation that anisole is a marginal solvent for P3HT at room temperature and also explains the propensity of P3HT to form ordered nanostructures in this solvent: the interactions between P3HT chains in anisole are just strong enough to allow chains to aggregate at room temperature, but weak enough that the chain segments do not become kinetically trapped in disordered metastable minima before reaching ordered global minimum energy structures.

The persistence length was calculated using eqn (3) for the uncollapsed chains in the simulation with reduced P3HT–P3HT interactions at 293 K and found to be 7.5 ± 0.2 nm, similar to the values obtained for uncollapsed P3HT in anisole from the single-chain simulations in Section 4.1 at 323 K and 353 K. The width of the multi-chain aggregates of ≈50 nm in the simulations of P3HT in anisole at 293 K provide an estimate for the persistence length of P3HT in the aggregated state. Thus the persistence length increases by an order-of-magnitude upon aggregation due to the formation of the ordered lamellar structures in the aggregated state.

4.3 Implications for electronic properties

The increased order in the polymer chain due to aggregation has consequences for electronic properties. A simple estimate of the conjugation length of P3HT can be obtained by assuming that P3HT is broken into electronically isolated units (chromophores) if the inter-monomer dihedral angle exceeds a particular threshold value. Following previous estimates of conjugation lengths in simulations of P3HT,[18,52] a threshold value of 40° was chosen, above which quantum calculations have shown that electronic properties become significantly different from the coplanar monomer case.[53] The calculated distributions of conjugation lengths for unaggregated P3HT in the simulations with reduced P3HT–P3HT interactions and for multi-chain aggregates in anisole at 293 K are shown in Fig. 10. Aggregation of P3HT was found to result in increased planarisation of the polymer chains, with the average conjugation length increasing significantly upon

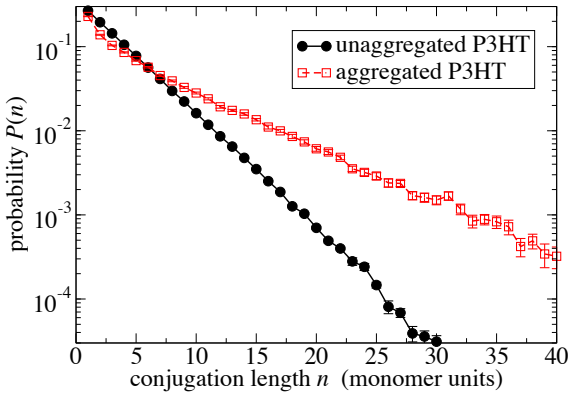

Fig. 10 Distribution of conjugation lengths in unaggregated and aggregated P3HT from simulations at 293 K.

aggregation from 3.7 to 6.0 monomer units. We have estimated the consequences of this increased planarisation of P3HT with aggregation on the UV-vis absorption spectrum by assuming that absorption by the chromophores in P3HT follows the same behaviour as that measured experimentally for thiophene oligomers as a function of length.[54] Fitting the energy of the experimental absorption maximum E (in eV, measured in dichloromethane) versus oligomer length n (in monomer units) to $E = 2.234 + 3.723/n$ and assuming linear scaling of the square of the transition dipole moment with chromophore length,[55] the absorption maximum can be estimated as the peak of the function $n(E)P(E) = nP(n)/|\mathrm{d}E/\mathrm{d}n|$, where $P(E)$ and $P(n)$ are the probability distributions of chromophores as a function of energy E and of length n, respectively. Using the conjugation length distributions for aggregated and unaggregated P3HT from our simulations, this analysis predicts a red shift in the absorption maximum $E_{\max}$ of 0.24 eV (from 2.65 eV to 2.41 eV), which compares reasonably well with the experimental red shift of 0.34 eV (from 2.77 eV to 2.43 eV) from unaggregated P3HT in THF to P3HT nanofibres in anisole at room temperature (see Supplementary Information). While full quantitative agreement with experimental results would require a more rigorous treatment of the electronic structure of P3HT,[56] this simple analysis demonstrates that the increased planarisation of P3HT chains upon aggregation makes a substantial contribution to changes in the absorption spectrum of P3HT and also provides further experimental validation of the coarse-grained P3HT model.

Many aspects of the electronic properties of P3HT nanofibres are still not well understood, including the observation of both H- and J-aggregate spectral features in a single nanofibre.[57] The calculations above illustrate how physically accurate coarse-grained simulation models can elucidate the molecular-level structural origins of electronic properties of self-assembled conjugated polymer nanostructures. The

coarse-grained P3HT model developed in this work, if coupled to a more sophisticated electronic model[58,59] allowing morphological effects on excitonic coupling and exciton migration to be investigated, could address these open questions, since it is sufficiently computationally efficient to simulate the formation of structural domains of the size observed in nanofibres,[8] but also retains sufficient molecular-scale detail to describe intra- and inter-chain coupling.

5 Conclusions

In conclusion, a coarse-grained simulation model of poly(3-hexylthiophene) (P3HT) in implicit anisole solvent was systematically parametrised by matching the local structure and dynamics in simulations of the model with that measured in simulations of an atomistic model. The coarse-grained model made it possible to simulate experimentally relevant polymer chain lengths and solution concentrations. The coarse-grained model was used to investigate the mesoscale structure and dynamics of P3HT in anisole, a solvent in which P3HT is known to self-assemble into high-aspect-ratio nanofibres when a solution of the polymer is cooled from elevated temperatures to room temperature. P3HT nanofibres were also prepared experimentally and characterised by atomic force microscopy and UV-vis spectroscopy. The coarse-grained simulations were found to agree well with experiments for the temperature dependence of aggregation of P3HT in anisole and for structural properties of P3HT aggregates such as nanofibre widths. At infinite dilution at 293 K, single P3HT chains were found to collapse to form two distinct nano-scale aggregate morphologies, namely hairpins and helices. Nucleation of hairpin structures, which are the precursors of nanofibres formed experimentally, was shown to be favoured energetically under these conditions. At 293 K and experimental concentrations, P3HT was found to form multi-chain aggregates comprising interleaved hairpin-structured chains. These aggregates were found to grow predominantly in the [010] π-stacking direction, with individual chains forming loops in the same (100) plane. The minimum curvature diameter of the chain loops at the sides of the aggregates was several times larger than the spacing between π-stacks. Consequently, adjacent chain segments in the π-stacking direction must generally belong to different chains. Aggregation was shown to result in significant planarisation of the P3HT chain, which has consequences for the polymer's conjugation length and electronic properties.

6 Acknowledgements

Financial support from The University of Adelaide is gratefully acknowledged. This work was supported by an award under the Merit Allocation Scheme on the NCI National Facility at the ANU and used computational resources of eResearch SA. The authors would also like to thank A. J. Moulé, R. Faller, and J. D. Roehling for fruitful discussions and K. Neubauer for assistance with the AFM measurements.

References

1 C. J. Brabec, M. Heeney, I. McCulloch and J. Nelson, *Chem. Soc. Rev.*, 2011, **40**, 1185–1199.
2 F. S. Kim, G. Ren and S. A. Jenekhe, *Chem. Mater.*, 2011, **23**, 682–732.
3 M. T. Dang, L. Hirsch and G. Wantz, *Adv. Mater.*, 2011, **23**, 3597–3602.
4 K. J. Ihn, J. Moulton and P. Smith, *J. Polym. Sci., Part B: Polym. Phys.*, 1993, **31**, 735–742.
5 S. Malik and A. K. Nandi, *J. Polym. Sci., Part B: Polym. Phys.*, 2002, **40**, 2073–2085.
6 S. Samitsu, T. Shimomura, S. Heike, T. Hashizume and K. Ito, *Macromolecules*, 2008, **41**, 8000–8010.
7 W. D. Oosterbaan, V. Vrindts, S. Berson, S. Guillerez, O. Douheret, B. Ruttens, J. D'Haen, P. Adriaensens, J. Manca, L. Lutsen and D. Vanderzande, *J. Mater. Chem.*, 2009, **19**, 5424–5435.
8 J. D. Roehling, I. Arslan and A. J. Moule, *J. Mater. Chem.*, 2012, **22**, 2498–2506.
9 S. Berson, R. De Bettignies, S. Bailly and S. Guillerez, *Adv. Funct. Mater.*, 2007, **17**, 1377–1384.
10 H. Xin, F. S. Kim and S. A. Jenekhe, *J. Am. Chem. Soc.*, 2008, **130**, 5424–5425.
11 H. Xin, G. Ren, F. S. Kim and S. A. Jenekhe, *Chem. Mater.*, 2008, **20**, 6199–6207.
12 H. Xin, O. G. Reid, G. Ren, F. S. Kim, D. S. Ginger and S. A. Jenekhe, *ACS Nano*, 2010, **4**, 1861–1872.
13 J. S. Kim, J. H. Lee, J. H. Park, C. Shim, M. Sim and K. Cho, *Adv. Funct. Mater.*, 2011, **21**, 480–486.
14 J. A. Merlo and C. D. Frisbie, *J. Phys. Chem. B*, 2004, **108**, 19169–19179.
15 F. C. Grozema, P. T. van Duijnen, Y. A. Berlin, M. A. Ratner and L. D. A. Siebbeles, *J. Phys. Chem. B*, 2002, **106**, 7791–7795.
16 D. L. Cheung, D. P. McMahon and A. Troisi, *J. Phys. Chem. B*, 2009, **113**, 9393–9401.
17 B. Meredig, A. Salleo and R. Gee, *ACS Nano*, 2009, **3**, 2881–2886.
18 M. Bernardi, M. Giulianini and J. C. Grossman, *ACS Nano*, 2010, **4**, 6599–6606.
19 C. Melis, A. Mattoni and L. Colombo, *J. Phys. Chem. C*, 2010, **114**, 3401–3406.
20 C. Melis, L. Colombo and A. Mattoni, *J. Phys. Chem. C*, 2011, **115**, 576–581.
21 M. I. Saba, C. Melis, L. Colombo, G. Malloci and A. Mattoni, *J. Phys. Chem. C*, 2011, **115**, 9651–9655.
22 T. Adachi, J. Brazard, R. J. Ono, B. Hanson, M. C. Traub, Z.-Q. Wu, Z. Li, J. C. Bolinger, V. Ganesan, C. W. Bielawski, D. A. Vanden Bout and P. F. Barbara, *J. Phys. Chem. Lett.*, 2011, **2**, 1400–1404.
23 D. Reith, M. Pütz and F. Müller-Plathe, *J. Comput. Chem.*, 2003, **24**, 1624–1636.
24 S. Izvekov and G. A. Voth, *J. Chem. Phys.*, 2005, **123**, 134105–13.
25 D. M. Huang, R. Faller, K. Do and A. J. Moulé, *J. Chem. Theory Comput.*, 2010, **6**, 526–537.
26 C.-K. Lee, C.-W. Pao and C.-W. Chu, *Energy Environ. Sci.*, 2011, **4**, 4124–4132.
27 C.-K. Lee and C.-W. Pao, *J. Phys. Chem. C*, 2012, **116**, 12455–12461.
28 V. Marcon and G. Raos, *J. Am. Chem. Soc.*, 2006, **128**, 1408–1409.
29 W. L. Jorgensen, D. S. Maxwell and J. Tirado-Rives, *J. Am. Chem. Soc.*, 1996, **118**, 11225–11236.
30 S. B. Darling and M. Sternberg, *J. Phys. Chem. B*, 2009, **113**, 6215–6218.

31 W. L. Jorgensen and N. A. McDonald, *THEOCHEM*, 1998, **424**, 145–155.
32 Sigma-Aldrich Catalog: http://www.sigmaaldrich.com.
33 M. L. P. Price, D. Ostrovsky and W. L. Jorgensen, *J. Comput. Chem.*, 2001, **22**, 1340–1352.
34 S. J. Plimpton, *J. Comput. Phys.*, 1995, **117**, 1–19.
35 W. Humphrey, A. Dalke and K. Schulten, *J. Mol. Graph.*, 1996, **14**, 33–38.
36 J. P. Ryckaert, G. Ciccotti and H. J. C. Berendsen, *J. Comput. Phys.*, 1977, **23**, 327–341.
37 R. W. Hockney and J. W. Eastwood, *Computer Simulation Using Particles*, Taylor & Francis, Bristol, 1988.
38 S. J. Plimpton, R. Pollock and M. Stevens, Proceedings of the Eighth SIAM Conference on Parallel Processing for Scientific Computing, Minneapolis, MN, 1997.
39 M. P. Allen and D. J. Tildesley, *Computer Simulation of Liquids*, Clarendon, Oxford, 1987.
40 T. Schneider and E. Stoll, *Phys. Rev. B*, 1978, **17**, 1302–1322.
41 R. Faller and D. Reith, *Macromolecules*, 2003, **36**, 5406–5414.
42 M. Chiu, T. W. Kee and D. M. Huang, *Aust. J. Chem.*, 2012, **65**, 463–471.
43 D. Chandler, *Introduction to Modern Statistical Mechanics*, Oxford University Press, Oxford, 1987.
44 D. Reith, B. Müller, F. Müller-Plathe and S. Wiegand, *J. Chem. Phys.*, 2002, **116**, 9100–9106.
45 T. Chen, A.-P. Hynninen, R. K. Prud'homme, I. G. Kevrekidis and A. Z. Panagiotopoulos, *J. Phys. Chem. B*, 2008, **112**, 16357–16366.
46 C. K. Lee, C. C. Hua and S. A. Chen, *J. Phys. Chem. B*, 2008, **112**, 11479–11489.
47 W. F. van Gunsteren and H. J. C. Berendsen, *Mol. Phys.*, 1982, **45**, 637–647.
48 N. Kiriy, E. Jähne, H.-J. Adler, M. Schneider, A. Kiriy, G. Gorodyska, S. Minko, D. Jehnichen, P. Simon, A. A. Fokin and M. Stamm, *Nano Lett.*, 2003, **3**, 707–712.
49 M. Rubinstein and R. H. Colby, *Polymer Physics*, Oxford University Press, Oxford, 2003.
50 G. W. Heffner and D. S. Pearson, *Macromolecules*, 1991, **24**, 6295–6299.
51 D. H. Kim, Y. D. Park, Y. Jang, S. Kim and K. Cho, *Macromol. Rapid Commun.*, 2005, **26**, 834–839.
52 N. Vukmirović and L. W. Wang, *J. Phys. Chem. B*, 2009, **113**, 409–415.
53 J. L. Bredas, G. B. Street, B. Themans and J. M. Andre, *J. Chem. Phys.*, 1985, **83**, 1323–1329.
54 J. Gierschner, J. Cornil and H. J. Egelhaaf, *Adv. Mater.*, 2007, **19**, 173–191.
55 B. Kohler and I. Samuel, *J. Chem. Phys.*, 1995, **103**, 6248.
56 F. C. Spano, *Annu. Rev. Phys. Chem.*, 2006, **57**, 217–243.
57 M. Baghgar, J. Labastide, F. Bokel, I. Dujovne, A. McKenna, A. M. Barnes, E. Pentzer, T. Emrick, R. Hayward and M. D. Barnes, *J. Phys. Chem. Lett.*, 2012, **3**, 1674–1679.
58 H. Yamagata and F. C. Spano, *J. Chem. Phys.*, 2012, **136**, 184901–14.
59 O. R. Tozer and W. Barford, *J. Phys. Chem. A*, 2012, **116**, 10310–10318.